PAPER

Terahertz wave manipulation through coupling of spoof plasmonics and Fabry–Perot resonance

IOP Publishing Journal of Physics D: Applied Physics
J. Phys. D: Appl. Phys. **51** (2018) 405101 (8pp) https://doi.org/10.1088/1361-6463/aad89f

Terahertz wave manipulation through coupling of spoof plasmonics and Fabry–Perot resonance

Baoshan Guo[1], Lan Jiang[1,4], Yanhong Hua[1], Xin Li[1], Tianhong Cui[2] and YongFeng Lu[3]

[1] Laser Micro/Nano Fabrication Laboratory, School of Mechanical Engineering, Beijing Institute of Technology, Beijing 100081, People's Republic of China
[2] Department of Mechanical Engineering, University of Minnesota, Minneapolis, MN, 55455, United States of America
[3] Department of Electrical Engineering, University of Nebraska-Lincoln, Lincoln, NE 68588-0511, United States of America

E-mail: jianglan@bit.edu.cn

Received 11 April 2018, revised 30 July 2018
Accepted for publication 7 August 2018
Published 24 August 2018

Abstract

The 'trapped rainbow' mechanism of graded gratings has been demonstrated only as a type of groove reflection. In this study, we investigate the physical mechanism of the 'trapped rainbow' and demonstrate that a small step increase (~1/50λ) in the depth of a single obstructed groove can terminate the propagation of surface terahertz (THz) waves and reflect them back. A single obstructed groove can easily manipulate the properties of THz waves by changing the depth or the refractive index of the groove because the cutoff frequency is highly sensitive to the property of the groove. In addition, waves transmitted and reflected by a single groove can be controlled periodically over a period of a 1/2 − λ increase in depth owing to the interference of surface spoof plasmonics and Fabry–Perot resonance. This is an easy means of controlling surface THz waves and fabricating more compact integrated optical devices such as THz branch waveguides, band pass filters, reflectors, and splitters.

Keywords: plasmonics, metamaterial, trapped rainbow, THz

(Some figures may appear in colour only in the online journal)

1. Introduction

A major driving force in the plasmonics domain is the ability to spatially confine electromagnetic (EM) energy at visible frequencies over distances significantly smaller than the wavelength; this ability can facilitate the development of many promising applications related to the miniaturization of photonic circuits [1, 2], near-field optics and microscopy [3, 4], biological sensors [5, 6], and photovoltaics [7, 8]. Surface plasmon polaritons (SPPs) and localized surface plasmons (LSPs) at metal–dielectric interfaces have unlocked a previously inaccessible length of scale by exploiting their own subwavelength nature. At a more fundamental level, both LSPs and SPPs can enhance light–matter interaction on the subwavelength scale [9, 10]. In the currently nascent stages, usage of SPPs and LSPs is limited to visible or near-infrared frequencies because their subwavelength confinement relies on the penetration of the EM field into metal. At lower frequencies such as terahertz (THz) frequencies, metals behave akin to perfect conductors (PECs), which do not support surface plasmons [11]. To extend the advantageous properties of surface plasmons to low frequencies (far infrared, THz, or microwave), periodic perforated plane surfaces and a variety of structured waveguide configurations based on spoof SPPs (SSPPs) have been developed to achieve subwavelength confinement in metal gratings at low frequencies [12, 13]. In this manner, confinement does not rely on the finite conductivity of the metal but rather on its surface structure [12, 13].

[4] Author to whom any correspondence should be addressed.

Similar to SSPs, SSPPs are sensitive to surface properties; for example, different surface structures or material interfaces can significantly change the transmitted or propagated EM fields [14–20]. Based on this property, SSPPs enable the application of THz waves in many promising fields such as THz sensing [21], THz imaging [22], THz spectroscopy [23], THz communication [24], and THz biosensing [25], with unprecedented sensitivity.

1D periodic grating on a metal surface has been used as a typical SSPP waveguide [13, 26, 27]. The properties of SSPPs are insensitive to waveguide thickness, which provides great flexibility and practicability in fabrication [28–31]. In previous studies, SSPP waveguides with rectangular, slanted rectangular, trapezoidal, V-shaped, and half-moon grooves have been proposed and studied both theoretically and experimentally because groove shape apparently influences the field confinement of SSPPs [32–34]. In addition, surface gratings with graded depth [35–39], graded period [40], and upright or downward pyramidal grooves [41] have been used to trap surface waves—an effect known as 'trapped rainbow'. In all the aforementioned studies, the physical mechanism of the 'trapped rainbow' has been thought to be that the wave vector can gradually be increased to an infinite value because of the gradually increasing groove depth or width, which eventually decreases the group velocity of the surface waves to zero.

We demonstrated that the aforementioned common understanding is not completely accurate, and that the physical origin of the 'trapped rainbow' is merely a type of reflection as opposed to real wave trapping [42]. However, detailed understanding of the physical mechanism underlying single-groove reflection has not been reported. In this paper, we extend this theory further and reveal that the transmission or reflection of surface waves can be controlled by a single groove of varying depth or refractive index of the media. The transmission or reflection property shows a clear periodical change as the obstructed groove depth increases; this is caused by the interference of surface modes and waveguide modes excited in the very narrow slit. The standing THz surface waves formed on the grating surface have considerably higher intensities, which can be used to develop applications such as surface sensing and imaging.

2. Simulation and discsion

A grating with rectangular grooves perforated on a metal surface is governed by three main parameters: depth (d), width (w), and period (p). Such a simple grating can be designed to propagate and decelerate EM waves of varying frequency simply by tuning the main parameters. For p-polarized (Ex, Ez, Hy) EM waves propagating along a surface grating (figure 1(b)), the dispersion relationship is determined by the aforementioned three main parameters and expressed as follows [11, 13]:

$$\beta = \frac{\omega}{c}\sqrt{1 + \frac{w^2}{p^2}\tan^2\left(\frac{\omega}{c}d\right)} \qquad (1)$$

where c is the velocity of light in a vacuum, β is the wave vector, and ω is the angular frequency. The cutoff frequency estimated using equation (1) is slightly higher than that obtained through finite difference time domain (FDTD) simulation because equation (1) is a simplified equation. To obtain a more precise prediction, an eigenvalue equation of the corrugated conducting plane of a periodic system must be introduced, and scattering components of a higher order must be considered [11, 13, 43]. A grating structure for THz waves is designed in this study. The conclusion is applicable for other frequencies, just as various EM frequencies exhibit the 'trapped rainbow' phenomenon.

Through equation (1), the theoretical or analytical results of the dispersion curves of a surface grating can be obtained (figure 1(a)). The period (p) equals 20 μm and the width (w) is half of the period (p). When the depth $d = 5$ μm (red curve in figure 1(a)), the cutoff frequency is higher than 10 THz, and thus the grating can support propagated modes below 10 THz. As the grating depth increases, the cutoff frequency decreases. When $d = 10$ μm (blue curve in figure 1(a)), the cutoff frequency decreases to approximately 6.5 THz. When the depth is increased to 15 μm (green curve in figure 1(a)) and 20 μm (pink curve in figure 1(a)), the cutoff frequency decreases to approximately 4.5 and 3.5 THz, respectively.

To validate the aforementioned theoretical results, a grating model (figure 1(c)) is built and simulated using the FDTD method. The FDTD simulation region is surrounded by a perfectly matched absorbing layer with a uniform cell of $\Delta x = \Delta z = 1$ μm. A p-polarized (Hy, Ex, Ez) pulsed wave is introduced as an end fire excitation source to excite the surface THz waves. The frequency of the pulse source ranges from 1 to 7 THz (black curve in figure 1(b)). The metal in the simulation is modeled as a PEC. According to the FDTD simulation results (figure 1(b)), the cutoff frequencies of such a grating of depth $d = 5$ μm (red curve), 10 μm (blue curve), 15 μm (green curve), and 20 μm (pink curve) are approximately 7, 4.7, 3.8, and 2.9 THz, respectively, all of which are lower than the theoretical results, especially those for the shallow grooves. We can see the intensity jump from zero to the higher intensity of the source in figure 1(b), and the jump region is very narrow only about 0.1 THz. To maintain consistency, when we read the cut-off frequency from the FDTD simulation as shown in figure 1(b), we took the point of strength equal to '0.1' as the cut-off frequency in the intensity jump region. For the theoretical results shown in figure 1(a), we took the cutoff frequencies when the slope of tangent of the dispersion curve goes to zero. A comparison of the cutoff frequencies of various grating depths acquired using equation (1) and through simulation is shown in figure 1(d). The theoretical results (black dots) exhibit the same trend as the simulation results (red dots), albeit with a shift to higher frequencies at all data points. This frequency mismatch is more apparent for the shallow grooves. If the grating depth is increased, groove cavity modes of a higher order appear [30, 44]; this could be why the mismatch between the theoretical and simulation results decreases as the groove depth increases. For groove depths greater than 20 μm, two propagation modes coexist,

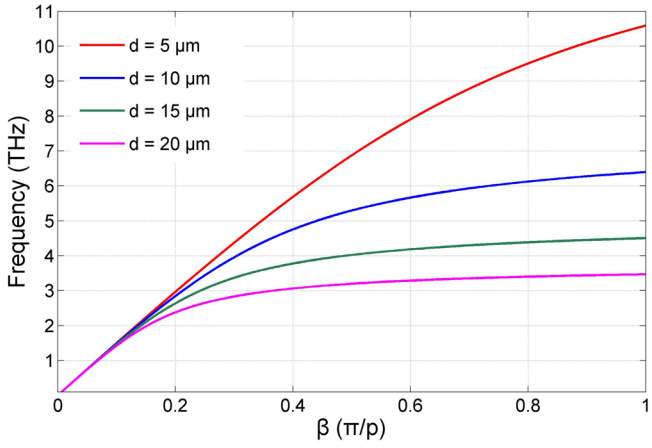

(a)

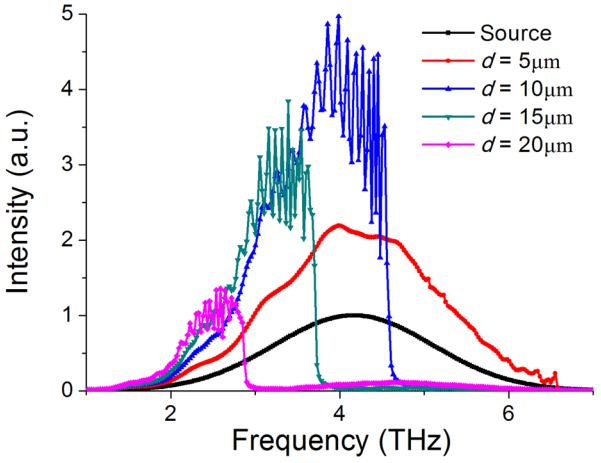

(b)

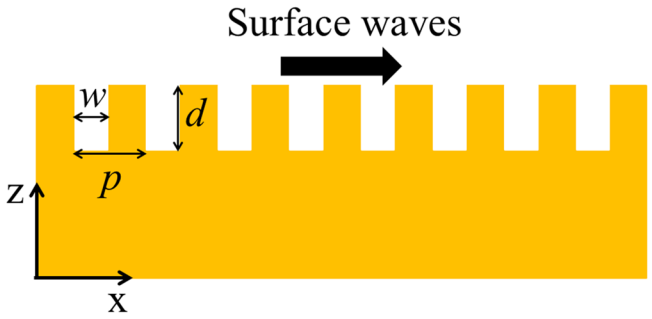

(c)

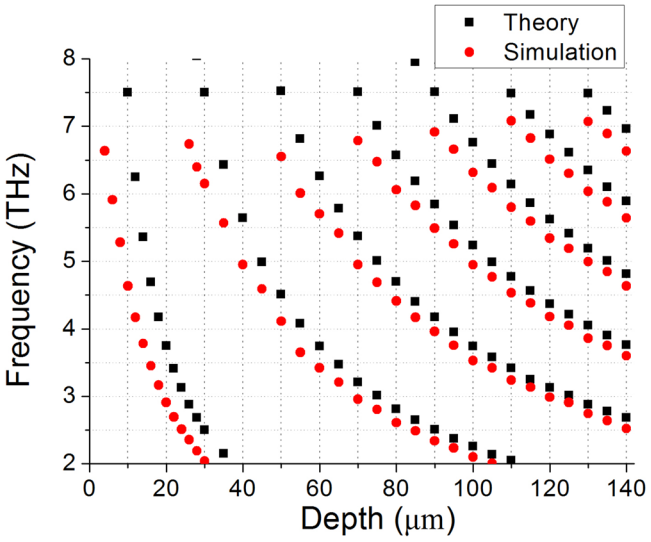

(d)

Figure 1. (a) Dispersion curves of gratings of varying depth (d) calculated using equation(1). When $d = 5$ μm (red line), the cutoff frequency is higher than 10 THz. When $d = 10$ μm (blue line), the cutoff frequency is approximately 6.5 THz. The cutoff frequency decreases to 4.5 and 3.5 THz when d is increased to 15 μm (green line) and 20 μm (pink line), respectively. The grating period (p) and width (w) are 20 and 10 μm, respectively. (b) Simulation results of surface-propagated frequencies. The frequency of the source pulse ranges from 1 to 7 THz (black line). The propagated frequencies for various grating depths are represented by the red curve ($d = 5$ μm), blue curve ($d = 10$ μm), green curve ($d = 15$ μm), and pink curve ($d = 20$ μm). (c) Schematic of metal grating showing width (w), period (p), and depth (d). The surface waves propagate along the direction of the X axis. (d) Cutoff frequencies of various grating depths calculated using equation (1) (black dots) and through simulation (red dots). The theoretical results obtained using equation (1) (black dots) indicate shifting to higher frequencies relative to the simulation results (red dots); however, the trends of the two sets of results are the same. Modes of a higher order appear as the groove depth increases.

and thus two propagation bands and two corresponding cutoff frequencies are present. For groove depths equal to or greater than 70 μm and equal to 130 μm, the number of propagation modes increases to three and five, respectively. To reduce the simulation time, the groove depth increment during calculation and simulation of the cutoff frequencies is set to 2 μm for groove depths lower than 30 μm and increased to 5 μm for groove depths greater than 30 μm.

According to the dispersion curves, only the frequencies near the cutoff frequency have considerable wave vectors (β), and thus only these frequencies can be trapped by the grating. For a typical graded-depth grating, the propagated surface waves gradually approach the cutoff frequency of the deeper grooves during propagation. Hence, gratings with graded depth or period are used to gradually increase the wave vector (β) and trap the surface waves (known as 'trapped rainbow'). However, according to our simulation results, once the frequencies of the propagated modes are sufficiently close to the cutoff frequency, these frequencies are transformed from propagated modes to forbidden modes that cannot be further propagated, and they are reflected back even by a single deeper groove. Subsequently, the misleading 'trapping effect' appears [42].

Compared with a graded grating, a single groove offers a simple and compact method to manipulate EM waves. Only one deep groove is adequate to terminate the propagation of

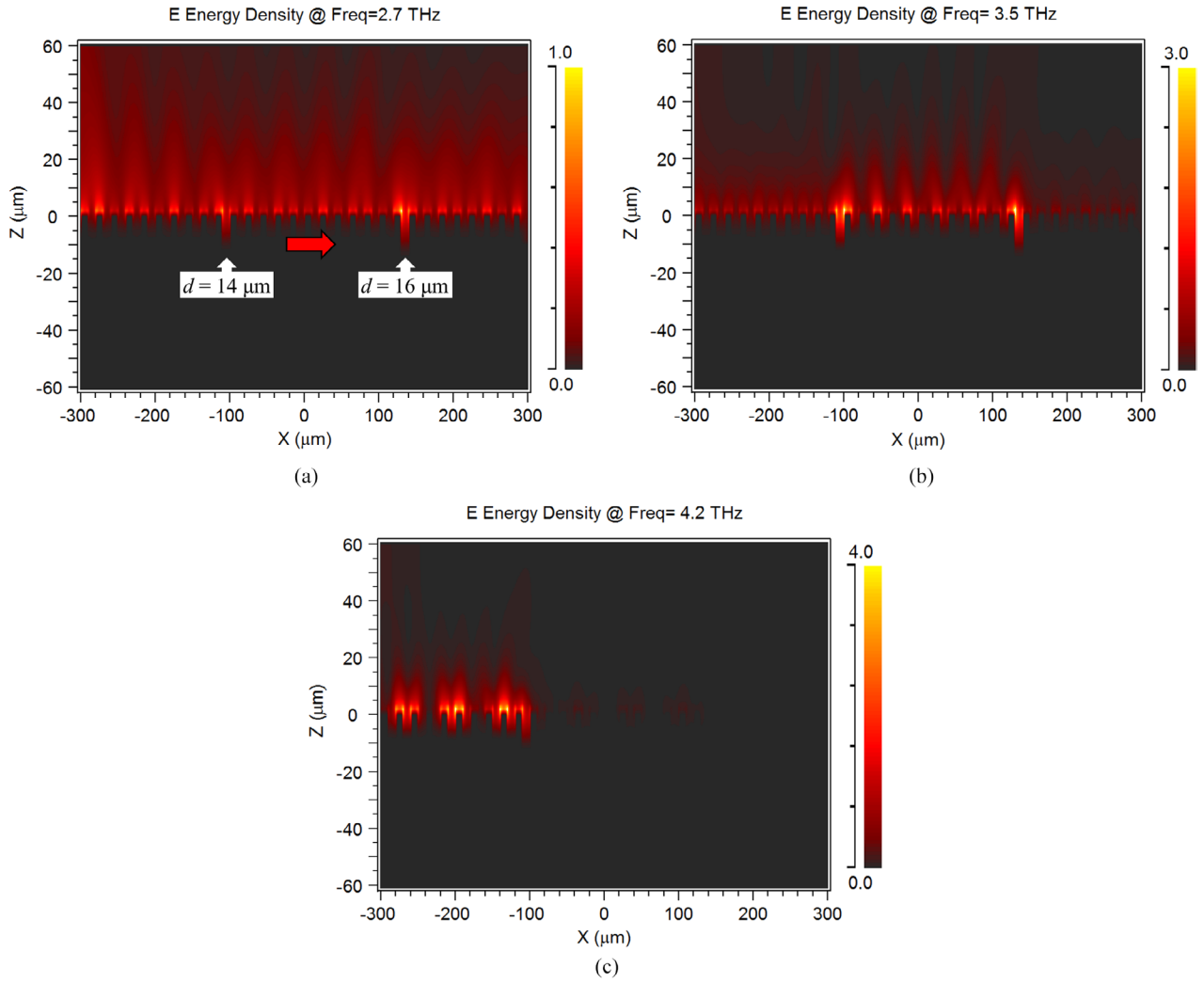

Figure 2. 2D EM field distributions of grating with two obstructed grooves as marked in (a) for different frequencies: (a) 2.7 THz; (b) 3.5 THz; and (c) 4.2 THz. A surface wave is propagated along the *X* direction. The depths of the two obstructed grooves are 14 and 16 μm.

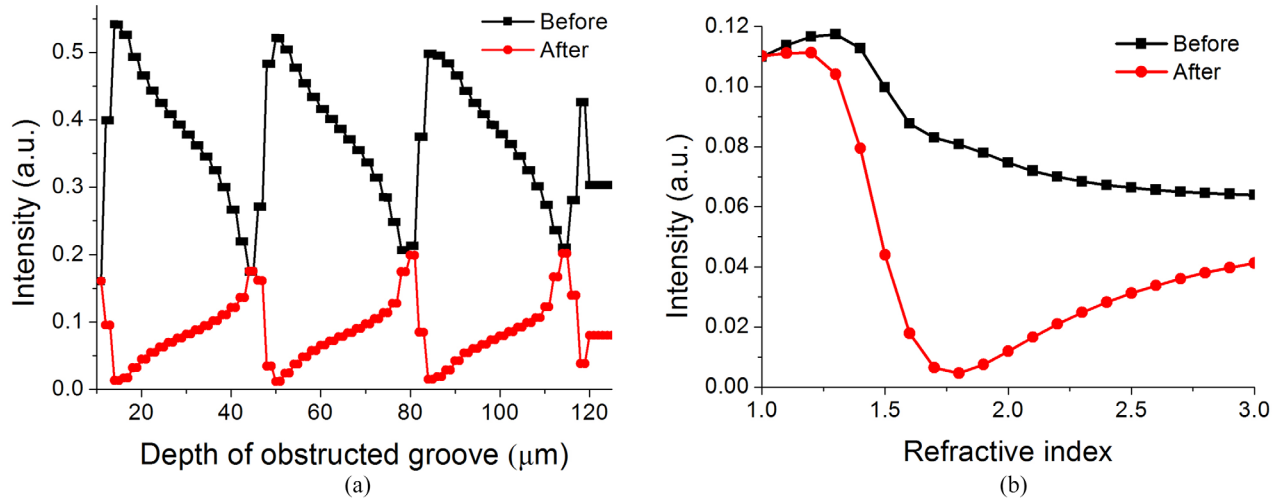

Figure 3. Intensity of surface waves before (black line) and after (red line) a single obstructed groove of varying depth, $n = 1$ (a) and various refractive indices, $d = 10$ μm (b).

surface waves and reflect them back. Furthermore, propagating surface THz waves are highly sensitive to grating depth. Herein, it is demonstrated that only a 2 μm (1/30–1/50λ) difference in the depth of a single obstructed groove can change the frequency of the blocking wave (figure 2).

Two obstructed grooves with depths of 14 and 16 μm were placed at two different positions on a grating with a period of 20 μm, width of 10 μm, and depth of 10 μm (figure 2(a)). The field distributions of EM waves with frequencies of 2.7, 3.5, and 4.2 THz are shown in figures 2(a)–(c), respectively. Such a grating has grooves of three depths (two obstructed grooves and one self-groove), denoting that three cutoff frequencies coexist. The 2.7 THz wave is below all cutoff frequencies and can propagate along the grating at all times (figure 2(a)). The 3.5 THz wave is above the cutoff frequency of the 16 μm-deep groove; therefore, it is blocked by the single 16 μm-deep groove (figure 2(b)). The 4.2 THz wave is above the cutoff frequencies of the 14 μm- and 16 μm-deep grooves and is blocked by the first single 14 μm groove (figure 2(c)). Accordingly, we concluded that a single groove with a small increase in depth can efficiently block surface waves with frequencies above its cutoff frequency.

Next, the blocking mechanism was investigated by changing the depth (figure 3(a)) and refractive index (figure 3(b)) of the single obstructed groove. The intensities of the 4.3 THz surface wave before (black curve) and after (red curve) the obstructed groove were recorded using two monitors placed on either side of the groove. The wave intensities before and after the obstructed groove reveal the reflection and transmission through the groove, respectively. In figure 3(a) (the medium in the groove is air, $n = 1$), the maximum reflected intensity corresponding to the minimum transmitted intensity appears when the depth of the obstructed groove equals 15, 50, and 85 μm. The maximum transmitted intensity appears when the depth of the obstructed groove equals 10, 45, and 80 μm. Here, the thickness of the metal film is 120 μm, and we do not investigate beyond this point. At depths greater than 120 μm, the groove is as deep as the metal film, and thus the reflected and transmitted intensities are no longer periodic as shown in figure 3(a). In addition, we demonstrated that the interaction between the surface modes and groove cavity modes leads to periodic changes in the intensity of surface waves. Therefore, the wave blocking effect changes periodically with the depth of a single obstructed groove when the groove cavity modes are present. The period of this change is approximately 35 μm, which is exactly half the wavelength of the 4.3 THz wave, denoting that the groove cavity modes can be ascribed to Fabry–Perot resonance.

If the simulation is repeated with a different wavelength such as 100 μm, the change period increases to 50 μm, which is half of the wavelength of 100 μm (the result is not shown). Therefore, the groove cavity mode is a key factor in determining the single-groove blocking effect. In addition, the refractive index of the media in the obstructed groove can change the behavior of the surface wave (figure 3(b)). Its effect on the transmission of the surface wave (red curve), especially from $n = 1.2$–1.8, is considerably stronger than that on the reflection (black curve). The lowest transmission can be achieved when $n = 1.8$. However, the reflection essentially continues to decrease as the refractive index increases, and thus a part of the surface wave is scattered out. To summarize, the propagation and reflection property of surface waves can be controlled easily by the single obstructed groove.

Figure 4 shows the surface wave distributions for frequency of 4.3 THz blocked by a single obstructed groove of varying depth. The depths of the obstructed groove are 10 μm (a), 45 μm (b), and 80 μm (c) corresponding to the maximum transmitted intensities in figure 3(a). Hence, all surface waves are transmitted smoothly. The depths of the obstructed groove are 15 μm (d), 50 μm (e), and 85 μm (f) corresponding to the maximum reflected intensities in figure 3(a). In this case, the single obstructed groove efficiently blocked most of the surface waves and reflected them back, and thus the wave intensity is considerably higher than that in the transmission case. Moreover, the percentage of reflection or transmission can be controlled by tuning the depth of the single obstructed groove. A 5 μm increase in the depth of the single groove can adjust the transmission from its highest point to its lowest point.

The propagation frequency curves of the corresponding obstructed groove depths are divided into two groups and shown in the upper and lower panels in figure 5. Within a certain narrow range of depth, the cutoff frequency shifts to a lower value as the groove depth increases (i.e. 10 to 15 μm, 45 to 50 μm, or 80 to 85 μm), similar to the case of the results shown in figure 1. However, this trend ceases to exist in the top panel or bottom panel of figure 5 when the depth increases in increments of 35 μm.

In the bottom panel of figure 5, the propagation frequencies of the obstructed groove with depths (d) of 10 μm (black curve), 45 μm (red curve), and 80 μm (blue curve) show that the transmission band is narrowed and modes of a higher order appear as d increases. However, the center position of the entire band shows no obvious shift. In fact, the center frequency or center wavelength of the transmission band is related to the Fabry–Perot resonance in the groove and can be estimated based on the groove depth: $d = n \cdot \lambda_{\text{center}}/2 + d_0$. Here, d and d_0 are the real groove depth and reference groove depth—which is considerably lower than the wavelength—respectively, and n is an integer (0, 1, 2, 3…). In our case, $d_0 = 10$ μm, and for the groove depths of 45 and 80 μm, the values of n are 1 and 2, respectively. Hence, their center wavelengths are all equal to 70 μm (~4.3 THz).

For the obstructed groove of depth (d) 15 μm (black curve), 50 μm (red curve), and 85 μm (blue curve) in the upper panel, the transmission band shows a different property. As the groove depth increases, the width of the transmission band decreases, whereas the center frequency shows a clear blue shift that is the complete opposite of the shift in figure 1. This can be ascribed to Fabry–Perot resonance. Similarly, the center frequency of the grooves of depths 50 (integer $n = 1$) and 85 (integer $n = 2$) μm can be calculated as 3.75 ($\lambda = 80$ μm) and 4 ($\lambda = 75$ μm) THz, respectively, showing an exact blue shift. In addition, a wave splitter can be realized by using a pair of obstructed grooves of depth 15 and 80 μm in different propagation directions. For example, a 3 THz wave can pass through by a 15 μm-deep groove but is blocked by

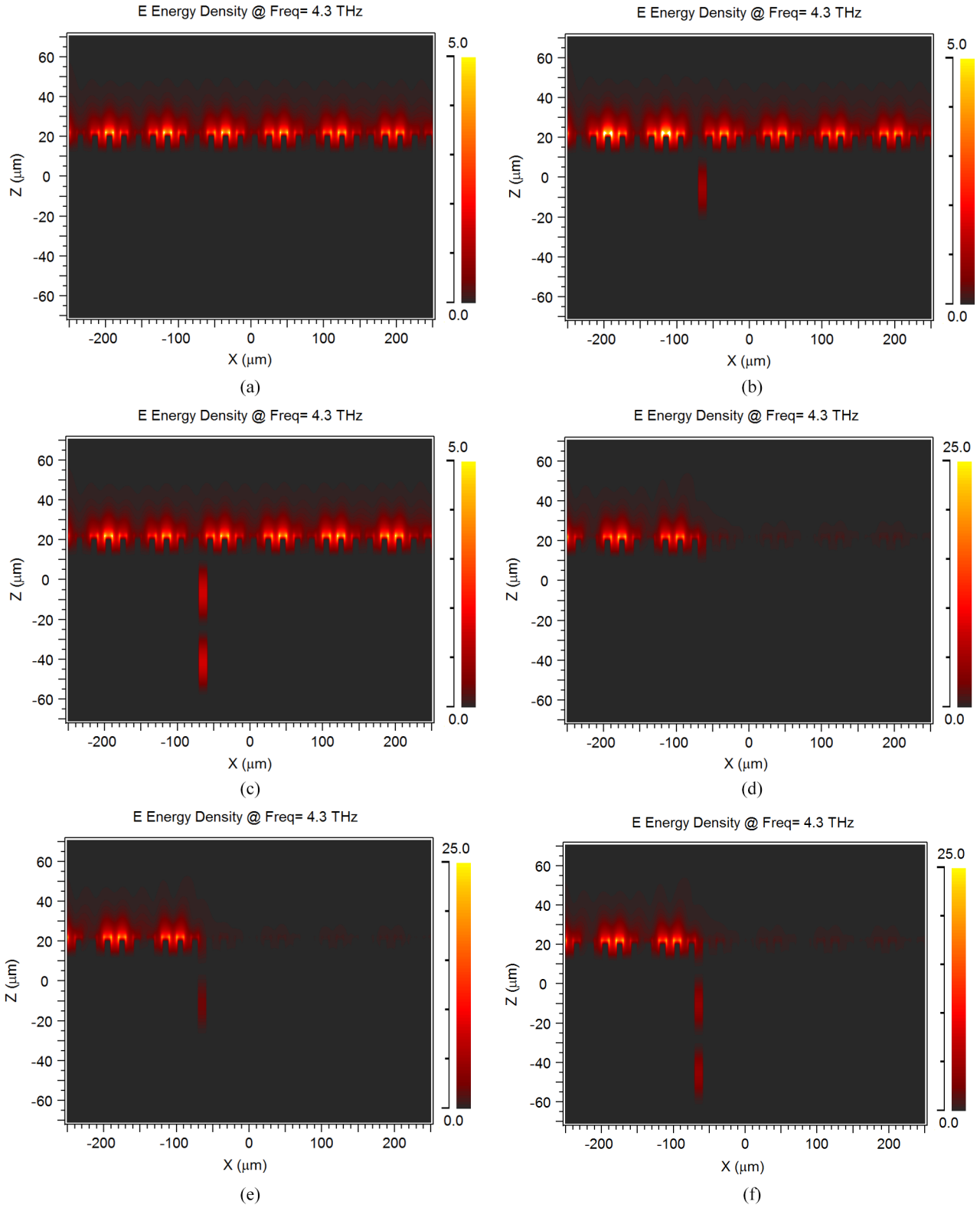

Figure 4. 2D field distribution of EM wave with a frequency of 4.3 THz obtained through grating with a single obstructed groove of varying depth. The depths of the obstructed groove are 10 μm (a), 45 μm (b), 80 μm (c), 15 μm (d), 50 μm (e), and 85 μm (f).

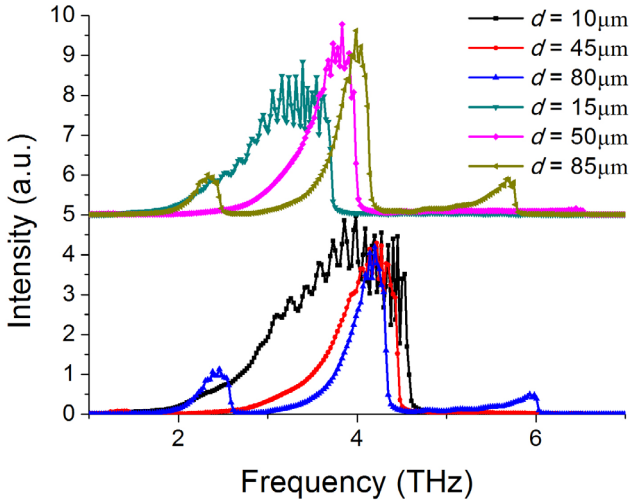

Figure 5. Propagated frequencies of surface waves for various groove depths. Lower panel: $d = 10$ μm (black curve), $d = 45$ μm (red curve), and $d = 80$ μm (blue curve). Upper panel: $d = 15$ μm (green curve), $d = 50$ μm (pink curve), and $d = 85$ μm (yellow curve).

an 80 μm-deep groove, and thus propagates along the direction of the 15 μm-deep groove. A 4 THz wave is blocked by a 15 μm-deep groove and can pass through an 80 μm-deep groove; thus, it propagates along the direction of the 80 μm-deep groove.

3. Conclusion

The analytical and numerical results of the grating cutoff frequency show a huge mismatch for shallow grooves ($d \ll \lambda$); this mismatch decreases gradually for deeper grooves that can support groove cavity modes. Because the cutoff frequency is sensitive to groove depth, only a 2 μm (1/30–1/50λ) increase in the depth of a single obstructed groove is sufficient to terminate the propagation of surface THz waves and reflect them back; this demonstrates that the 'trapped rainbow' of a graded grating is not surface THz wave trapping but merely surface wave reflection. The depth or media refractive index of a single obstructed groove can be changed to easily manipulate the properties of EM waves; the main physical factor underlying this phenomenon is the interference of SSPP modes and Fabry–Perot resonance in the groove. Hence, controlling surface THz waves and fabricating more compact integrated optical devices such as branch-slowing waveguides, band pass filters, surface wave switches, and reflectors is considerably easier. Furthermore, if the gain media exists in the grooves, a grating section designed with a proper depth can form a cavity to fabricate a laser or spaser of unrestricted frequency range.

Acknowledgments

This study was supported by the National Natural Science Foundation of China (NSFC) under Grant no. 61605140 and National Key R&D Program of China (2017YFB1104300).

ORCID iDs

Baoshan Guo https://orcid.org/0000-0002-9640-1532

References

[1] Barnes W L, Dereux A and Ebbesen T W 2003 Surface plasmon subwavelength optics *Nature* **424** 824–30
[2] Ozbay E 2006 Plasmonics: merging photonics and electronics at nanoscale dimensions *Science* **311** 189–93
[3] Kawata S, Inouye Y and Verma P 2009 Plasmonics for near-field nano-imaging and superlensing *Nat. Photon.* **3** 388–94
[4] Gramotnev D K and Bozhevolnyi S I 2010 Plasmonics beyond the diffraction limit *Nat. Photon.* **4** 83–91
[5] Anker J N, Hall W P, Lyandres O, Shah N C, Zhao J and Duyne R P V 2008 Biosensing with plasmonic nanosensors *Nat. Mater.* **7** 442–53
[6] Liu N, Mesch M, Weiss T, Hentschel M and Giessen H 2010 Infrared perfect absorber and its application as plasmonic sensor *Nano Lett.* **10** 2342–8
[7] Atwater H A and Polman A 2010 Plasmonics for improved photovoltaic devices *Nat. Mater.* **9** 205–13
[8] Schuller J A, Barnard E S, Cai W, Jun Y C, White J S and Brongersma M L 2010 Plasmonics for extreme light concentration and manipulation *Nat. Mater.* **9** 193–204
[9] Akimov A V, Mukherjee A, Yu C L, Chang D E, Zibrov A S, Hemmer P R, Park H and Lukin M D 2007 Generation of single optical plasmons in metallic nanowires coupled to quantum dots *Nature* **450** 402–6
[10] Trugler A and Hohenester U 2008 Strong coupling between a metallic nanoparticle and a single molecule *Phys. Rev.* B **77** 115403
[11] Maier S A, Andrews S R, Martin-Moreno L and Garcia-Vidal F J 2006 Terahertz surface plasmon-polariton propagation and focusing on periodically corrugated metal wires *Phys. Rev. Lett.* **97** 176805
[12] Pendry J B, Martin-Moreno L and Garcia-Vidal F J 2004 Mimicking surface plasmons with structured surfaces *Science* **305** 847–8
[13] Garcia-Vidal F J, Martin-Moreno L and Pendry J B 2005 Surfaces with holes in them: new plasmonic metamaterials *J. Opt. A: Pure Appl. Opt.* **7** S97
[14] Hibbins A P, Evans B R and Sambles J R 2005 Broadband spoof plasmons and subwavelength electromagnetic energy confinement on ultrathin metafilms *Science* **308** 670
[15] Shen L, Chen X and Yang T J 2008 Terahertz surface plasmon polaritons on periodically corrugated metal surfaces *Opt. Express* **16** 3326
[16] Maier S and Andrews S 2006 Terahertz pulse propagation using plasmon-polariton-like surface modes on structured conductive surfaces *Appl. Phys. Lett.* **88** 251120
[17] Johnston M B 2007 Plasmonics: superfocusing of terahertz waves *Nat. Photon.* **1** 14
[18] Guo B S, Song G F and Chen L H 2007 Plasmonic very-small-aperture lasers *Appl. Phys. Lett.* **91** 021103
[19] Guo B S, Song G F and Chen L H 2009 Resonant enhanced wave filter and waveguide via surface plasmons *IEEE Trans. Nanotechnol.* **8** 408
[20] Kats M A, Woolf D, Blanchard R, Yu N and Capasso F 2011 Spoof plasmon analogue of metal–insulator–metal waveguides *Opt. Express* **16** 14860
[21] Brucherseifer M, Nagel M, Haring Bolivar P, Kurz H, Bosserhoff A and Büttner R 2000 Label-free probing of the binding state of DNA by time-domain terahertz sensing *Appl. Phys. Lett.* **77** 4049

[22] Chan W L, Moravec M L, Baraniuk R G and Mittleman D M 2008 Terahertz imaging with compressed sensing and phase retrieval *Opt. Lett.* **33** 974–6
[23] Liu H B, Plopper G, Earley S, Chen Y Q, Ferguson B and Zhang X C 2007 Sensing minute changes in biological cell monolayers with THz differential time-domain spectroscopy *Biosens. Bioelectron.* **22** 1075–80
[24] Ibraheem I A, Krumbholz N, Mittleman D and Koch M 2008 Low-dispersive dielectric mirrors for future wireless terahertz communication systems *IEEE Microw. Wirel. Co. Lett.* **18** 67–9
[25] Nagel M, Haring Bolivar P, Brucherseifer M, Kurz H, Bosserhoff A and Buttner R 2002 Integrated THz technology for label-free genetic diagnostics *Appl. Phys. Lett.* **80** 154
[26] Shen L F, Chen X D and Yang T J 2008 Terahertz surface plasmon polaritons on periodically corrugated metal surfaces *Opt. Express* **16** 3326–33
[27] Wood J J, Tomlinson L A, Hess O, Maier S A and Fernández-Domínguez A I 2012 Spoof plasmon polaritons in slanted geometries *Phys. Rev.* B **85** 075441
[28] Martin-Cano D, Nesterov M L, Fernandez-Dominguez A I, Garcia-Vidal F J, Martin-Moreno L and Moreno E 2010 Domino plasmons for subwavelength terahertz circuitry *Opt. Express* **18** 754–64
[29] Martin-Cano D, Quevedo-Teruel O, Moreno E, Martin-Moreno L and Garcia-Vidal F J 2011 Waveguided spoof surface plasmons with deep-subwavelength lateral confinement *Opt. Lett.* **36** 4635–7
[30] Shen X P, Cui T J, Martin-Cano D and Garcia-Vidal F J 2013 Conformal surface plasmons propagating on ultrathin and flexible films *Proc. Natl Acad. Sci.* **110** 40–5
[31] Shen X P and Cui T J 2013 Planar plasmonic metamaterial on a thin film with nearly zero thickness *Appl. Phys. Lett.* **102** 211909
[32] Zhu F M, Zhang Y Y, Shen L F and Gao Z 2012 Subwavelength guiding of terahertz radiation by shallowly corrugated metal surfaces *J. Electromagn. Waves Appl.* **26** 120–9
[33] Xiang H, Meng Y, Zhang Q, Qin F F, Xiao J J, Han D Z and Wen W J 2015 Spoof surface plasmon polaritons on ultrathin metal strips with tapered grooves *Opt. Commun.* **356** 59–63
[34] Gao Z, Shen L F and Zheng X D 2012 Highly-confined guiding of terahertz waves along subwavelength grooves *IEEE Photonics Technol. Lett.* **24** 1343–5
[35] Gan Q, Fu Z, Ding Y J and Bartoli F J 2008 Ultrawide-bandwidth slow-light system based on THz plasmonic graded metallic grating structures *Phys. Rev. Lett.* **100** 256803
[36] Guo B S and Shi W 2014 Real propagation speed of the ultraslow plasmonic THz waveguide *Appl. Phys.* B **114** 503–7
[37] Guan C, Shi J, Ding M, Wang P, Hua P, Yuan L and Brambilla G 2013 In-line rainbow trapping based on plasmonic gratings in optical Microfibers *Opt. Express* **14** 16552
[38] Zeng C and Cui Y 2012 Rainbow trapping of surface plasmon polariton waves in metal–insulator–metal graded grating waveguide *Opt. Commun.* **290** 188–91
[39] Wang G, Lu H and Liu X 2012 Trapping of surface plasmon waves in graded grating waveguide system *Appl. Phys. Lett.* **101** 013111
[40] Guo B S, Shi W and Yao J Q 2015 Slowing and trapping THz waves system based on plasmonic graded period grating *J. Opt.* **45** 50–7
[41] Tian L, Liu J, Zhou K, Gao Y and Liu S 2016 Investigation of mechanism: spoof SPPs on periodically textured metal surface with pyramidal grooves *Sci. Rep.* **6** 32008
[42] Guo B S 2018 Revealing the truth about 'Trapped Rainbow' storage of terahertz waves in plasmonic grating *Plasmonics* **13** 933–8
[43] Zhang K and Li D 2008 *Electromagnetic Theory for Microwaves and Optoelectronics* (Berlin: Springer)
[44] Liu X, Feng Y, Zhu B, Zhao J and Jiang T 2013 High-order modes of spoof surface plasmonic wave transmission on thin metal film structure *Opt. Express* **21** 31155